Complex Variables and Elliptic Equations
Publication details, including instructions for authors and subscription information:
http://www.tandfonline.com/loi/gcov20

Recovery of a material parameter of a soft elastic layer

Jean-Philippe Groby [a], Erick Ogam [b], Armand Wirgin [b] & Yongzhi Xu [c]

[a] Laboratoire d'Acoustique de l'Université du Maine, Le Mans, France

[b] Laboratoire de Mécanique et d'Acoustique, UPR 7051 du CNRS, 31 Chemin Joseph Aiguier, Marseille 13009, France

[c] Department of Mathematics, University of Louisville, Louisville, Kentucky, USA

Available online: 23 Aug 2011

To cite this article: Jean-Philippe Groby, Erick Ogam, Armand Wirgin & Yongzhi Xu (2011): Recovery of a material parameter of a soft elastic layer, Complex Variables and Elliptic Equations, DOI:10.1080/17476933.2011.605449

To link to this article: http://dx.doi.org/10.1080/17476933.2011.605449

Complex Variables and Elliptic Equations
2011, 1–20, iFirst

Recovery of a material parameter of a soft elastic layer

Jean-Philippe Groby[a], Erick Ogam[b], Armand Wirgin[b*] and Yongzhi Xu[c]

[a]*Laboratoire d'Acoustique de l'Université du Maine, Le Mans, France;* [b]*Laboratoire de Mécanique et d'Acoustique, UPR 7051 du CNRS, 31 Chemin Joseph Aiguier, Marseille 13009, France;* [c]*Department of Mathematics, University of Louisville, Louisville, Kentucky, USA*

Communicated by Robert Gilbert

(*Received in final form 12 July 2011*)

We treat the inverse seismological problem of the recovery of the rigidity contrast from the temporal response on the ground (a flat stress-free surface) separating air from a homogeneous, isotropic, solid substratum overlain by a homogeneous, isotropic, solid layer (in contact with the ground) solicited by a shear-horizontal (SH) plane impulsive body wave incident in the substratum (a seismic solicitation whose sources are deep within the substratum). The forward-scattering analysis is first carried out in the frequency domain and subsequently in the time domain. A (complex eigenfrequency) method is elaborated for the computation of the time history and gives rise to the reliable numerical solutions for a large variety of configurations of interest in the geophysical setting under the hypothesis of non-dissipative, dispersionless media. The inverse-scattering analysis is carried out using the complex eigenfrequency method to generate synthetic data (predictor) as well as to constitute the theoretical model by which the data is inverted (estimator). The inverse crime is avoided by making one of the supposedly-known parameters (Γ) in the estimator different (from its counterpart γ) in the predictor. It is shown that the rigidity contrast is recovered with an accuracy that depends on the difference between Γ and γ.

Keywords: elastic layers; inverse scattering

AMS Subject Classifications: 65N21, 74H05, 74H45, 74J15, 74J20, 74J25

1. Introduction

This work is inspired by the oft-encountered problem of recovering the physical and geometric parameters of a typical geological structure and/or the parameters which characterize a seismic solicitation of the said structure. The geological structure considered herein consists of flat ground separating air from an underground constituted by a homogeneous, soft layer overlying, and in welded contact with, a homogeneous, hard, semi-infinite substratum. This configuration is assumed to be solicited by an impulsive SH plane body wave and the object at present is to recover

*Corresponding author. Email: wirgin@lma.cnrs-mrs.fr

ISSN 1747–6933 print/ISSN 1747–6941 online

DOI: 10.1080/17476933.2011.605449
http://www.informaworld.com

the rigidity contrast parameter from the time history of response on the ground to the seismic solicitation.

2. The forward-scattering problem

2.1. *Space-time and space-frequency formulations*

In the following, we shall be concerned with the determination of the vectorial displacement field $\mathbf{u}$ on, and underneath, the ground in response to a seismic solicitation. In general, $\mathbf{u}$ is a function of the spatial coordinates, incarnated in the vector $\mathbf{x}$ and time t, so that $\mathbf{u} = \mathbf{u}(\mathbf{x}, t)$.

We first carry out our analysis in the frequency domain, and thus search for $\mathbf{u}(\mathbf{x}, \omega)$, with ω the angular frequency. $\mathbf{u}(\mathbf{x}, t)$ and $\mathbf{u}(\mathbf{x}, \omega)$ are related by

$$\mathbf{u}(\mathbf{x}, t) = \int_{-\infty}^{\infty} \mathbf{u}(\mathbf{x}, \omega) \exp(-i\omega t) \mathrm{d}\omega, \tag{1}$$

wherein it should be noted that $\mathbf{u}(\mathbf{x}, \omega)$ is a generally-complex function, whereas $\mathbf{u}(\mathbf{x}, t)$ is a real function. The second step will therefore deal with the computation of the integral in (1).

2.2. *Frequency domain analysis of the reflection of a SH plane body wave from a stress-free planar boundary overlying a soft layer underlain by a hard substratum*

2.2.1. *Features of the problem*

Since everything is invariant with x_3, the analysis takes place in the $x_1 - x_2$ (sagittal) plane depicted in Figure 1.

In this figure: Γ_0 designates the (trace of the) interface between the substratum (half-space domain Ω_0) and the soft layer (laterally-unbounded domain Ω_1), and Γ_1 the (trace of the) flat ground. The medium $M^{[2]}$ above the latter is air, assumed to be the vacuum for the purpose of the analysis. The media in the layer and substratum

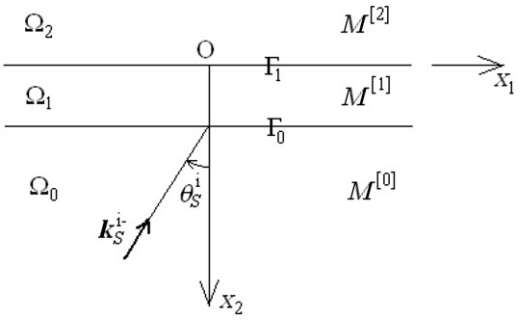

Figure 1. Cross-sectional view of the configuration of a stress-free flat surface overlying a soft layer (occupying domain Ω_1, filled with medium $M^{[1]}$) underlain by a hard solid substratum (occupying domain Ω_0, filled with medium $M^{[0]}$) submitted to a SH plane wave, propagating initially in the substratum.

are the elastic solids $M^{[1]}$ and $M^{[0]}$, respectively. This means that the constitutive parameters of these media are real constants (with respect to the frequency, i.e. the media are non-attenuating and dispersionless).

The incident plane wave propagates in Ω_0 toward the the interface Γ_0 and the ground Γ_1. Since the latter is stress-free (i.e. the normal and tangential components of traction are nil on the boundary), the total displacement field vanishes in the region Ω_2 above the boundary (Figure 1). One can always choose the cartesian coordinate system so that the wavevector associated with the incident shear wave (the subscript S will constitute a reminder that we deal with shear = transverse waves in the following) lies in the $x_1 - x_2$ plane. This is assumed herein and signifies that the displacement associated with this wave is perpendicular to the $x_1 - x_2$ plane and therefore lies in a horizontal plane. Thus, the incident wave is a shear wave and the associated displacement is horizontal; i.e. a shear-horizontal (SH) wave. Moreover, the motion associated with this wave is, due to the choice of the Cartesian reference system, independent of the coordinate x_3. This implies that the resultant total motion induced by this incident wave is independent of x_3, i.e. the boundary value problem is 2D, so that it is sufficient to look for the displacement field in the $x_1 - x_2$ plane. Actually, since we already know that the total displacement vanishes in the half plane above the boundary we must look for the total displacement field (hereafter designated by $\mathbf{u}^{[l]}(\mathbf{x}, \omega)$) only in Ω_0 and Ω_1.

Hereafter, we designate the density and Lamé parameters in Ω_l by $\rho^{[l]}$ and $\lambda^{[l]}$, $\mu^{[l]}$ (for $l = 0, 1$) respectively.

2.2.2. *Governing equations*

The mathematical translation of the boundary value problem in the *space-frequency domain* is

$$\mu u^{[l]}_{j,nn}(\mathbf{x}, \omega) + \left(\lambda^{[l]} + \mu^{[l]}\right) u^{[l]}_{n,nj}(\mathbf{x}, \omega) + \rho^{[l]} \omega^2 u^{[l]}_j(\mathbf{x}, \omega) = 0;$$
$$\forall \mathbf{x} = (x_1, x_2) \in \Omega_l;\ j = 1, 2, 3,\ l = 0, 1,\ n = 1, 2, \tag{2}$$

$$u^{[l]}_{j,3}(\mathbf{x}, \omega) = 0; \quad \forall \mathbf{x} \in \Omega_l;\ j = 1, 2, 3,\ l = 0, 1, \tag{3}$$

$$\left(\lambda^{[1]} + 2\mu^{[1]}\right) u^{[1]}_{2,2}(\mathbf{x}, \omega) + \lambda^{[1]} u^{[1]}_{1,1}(\mathbf{x}, \omega) = 0 \quad \text{on } \Gamma_1, \tag{4}$$

$$\mu^{[1]} u^{[1]}_{3,2}(\mathbf{x}, \omega) = \text{on} \quad \Gamma_1, \tag{5}$$

$$-\mu^{[1]}\left(u^{[1]}_{1,2}(\mathbf{x}, \omega) + u^{[1]}_{2,1}(\mathbf{x}, \omega)\right) = 0 \quad \text{on } \Gamma_1. \tag{6}$$

$$u^{[0]}_2(\mathbf{x}, \omega) = u^{[1]}_2(\mathbf{x}, \omega) \quad \text{on } \Gamma_0, \tag{7}$$

$$u^{[0]}_3(\mathbf{x}, \omega) = u^{[1]}_3(\mathbf{x}, \omega) \quad \text{on } \Gamma_0, \tag{8}$$

$$-u^{[0]}_1(\mathbf{x}, \omega) = -u^{[1]}_1(\mathbf{x}, \omega) \quad \text{on } \Gamma_0, \tag{9}$$

$$\left(\lambda^{[0]}+2\mu^{[0]}\right)u^{[0]}_{2,2}(\mathbf{x},\omega)+\lambda^{[0]}u^{[0]}_{1,1}(\mathbf{x},\omega)=\left(\lambda^{[1]}+2\mu^{[1]}\right)u^{[1]}_{2,2}(\mathbf{x},\omega)+\lambda^{[1]}u^{[1]}_{1,1}(\mathbf{x},\omega)\quad\text{on }\Gamma_0, \tag{10}$$

$$\mu^{[0]}u^{[0]}_{3,2}(\mathbf{x},\omega)=\mu^{[1]}u^{[1]}_{3,2}(\mathbf{x},\omega)\quad\text{on }\Gamma_0, \tag{11}$$

$$-\mu^{[0]}\left(u^{[0]}_{1,2}(\mathbf{x},\omega)+u^{[0]}_{2,1}(\mathbf{x},\omega)\right)=-\mu^{[1]}\left(u^{[1]}_{1,2}(\mathbf{x},\omega)+u^{[1]}_{2,1}(\mathbf{x},\omega)\right)\quad\text{on }\Gamma_0. \tag{12}$$

$$\begin{gathered}u^{[l]d}_j(\mathbf{x},\omega):=u^{[l]}_j(\mathbf{x},\omega)-\delta_{j0}u^i_j(\mathbf{x},\omega)\sim\text{outgoing waves;}\\ \|\mathbf{x}\|\to\infty,\quad \mathbf{x}\in\Omega_l,\ j=1,2,3,\ l=0,1,\end{gathered} \tag{13}$$

wherein $u^i_j(\mathbf{x},\omega)$ is the incident field, $u^{[l]d}_j(\mathbf{x},\omega)$ the (unknown) diffracted field in Ω_l, δ_{jk} the Kronecker delta symbol, and:

$$u^i_3(\mathbf{x},\omega)=A^{i-}_3\exp(i\mathbf{k}^{i-}_S\cdot\mathbf{x}),\quad u^i_1(\mathbf{x},\omega)=u^i_2(\mathbf{x},\omega)=0;\quad \forall\mathbf{x}\in\Omega_0, \tag{14}$$

$$\mathbf{k}^{i-}_S=(k^i_{S1},\ k^{i-}_{S2}),\quad k^i_{S1}=k^{[0]}_S\sin\theta^i_S,\quad k^{i-}_{S2}=-k^{[0]}_S\cos\theta^i_S,\quad k^{[0]}_S=\frac{\omega}{c^{[0]}_S}, \tag{15}$$

θ^i_S being the angle of incidence with respect to the x_2 axis and $c^{[l]}_S=\sqrt{\frac{\mu^{[l]}}{\rho^{[l]}}}$ the phase velocity of shear body waves in $M^{[l]}$.

Equation (2) is the space-frequency domain equation(s) of motion, (4)–(12) the boundary condition(s), (13) the radiation condition, and (14), (15) the description of the incident wave.

Until further notice, we drop the ω-dependence on all field quantities and consider it to be implicit.

2.2.3. *Field representations incorporating the radiation condition*

By the method of Helmholtz decomposition [1], and on account of the outgoing wave condition(s) (13), one can show that the following integral representations of the field are appropriate:

$$u^{[0]d}_1(\mathbf{x})=i\int_{-\infty}^{\infty}\left[\Phi^{[0]+}(k_1)k_1E\left(\mathbf{k}^{[0]+}_P\cdot\mathbf{x}\right)+\Psi^{[0]+}_3(k_1)k^{[0]+}_{S2}E\left(\mathbf{k}^{[0]+}_S\cdot\mathbf{x}\right)\right]\mathrm{d}k_1, \tag{16}$$

$$u^{[0]d}_2(\mathbf{x})=i\int_{-\infty}^{\infty}\left[\Phi^{[0]+}(k_1)k^{[0]+}_{P2}E\left(\mathbf{k}^{[0]+}_P\cdot\mathbf{x}\right)-\Psi^{[0]+}_3(k_1)k_1E\left(\mathbf{k}^{[0]+}_S\cdot\mathbf{x}\right)\right]\mathrm{d}k_1, \tag{17}$$

$$u^{[0]d}_3(\mathbf{x})=\int_{-\infty}^{\infty}\Xi^{[0]+}_3(k_1)E\left(\mathbf{k}^{[0]+}_S\cdot\mathbf{x}\right)\mathrm{d}k_1, \tag{18}$$

$$\begin{aligned}u^{[1]}_1(\mathbf{x})=u^{[1]d}_1(\mathbf{x})=i\int_{-\infty}^{\infty}&\left[\Phi^{[1]-}(k_1)k_1E\left(\mathbf{k}^{[1]-}_P\cdot\mathbf{x}\right)+\Psi^{[1]-}_3(k_1)k^{[1]-}_{S2}E\left(\mathbf{k}^{[1]-}_S\cdot\mathbf{x}\right)\right.\\&\left.+\Phi^{[1]+}(k_1)k_1\exp\left(i\mathbf{k}^{[1]+}_P\cdot\mathbf{x}\right)+\Psi^{[1]+}_3(k_1)k^{[1]+}_{S2}E\left(i\mathbf{k}^{[1]+}_S\cdot\mathbf{x}\right)\right]\mathrm{d}k_1,\end{aligned} \tag{19}$$

$$u_2^{[1]}(\mathbf{x}) = u_2^{[1]d}(\mathbf{x}) = i\int_{-\infty}^{\infty}\big[\Phi^{[1]-}(k_1)k_{P2}^{[1]-}E\big(\mathbf{k}_P^{[1]-}\cdot\mathbf{x}\big) - \Psi_3^{[1]-}(k_1)k_1E\big(\mathbf{k}_S^{[1]-}\cdot\mathbf{x}\big)$$
$$+\Phi^{[1]+}(k_1)k_{P2}^{[1]+}E\big(\mathbf{k}_P^{[1]+}\cdot\mathbf{x}\big) - \Psi_3^{[1]+}(k_1)k_1E\big(i\mathbf{k}_S^{[1]+}\cdot\mathbf{x}\big)\big]\mathrm{d}k_1, \quad (20)$$

$$u_3^{[1]}(\mathbf{x}) = u_3^{[1]d}(\mathbf{x}) = \int_{-\infty}^{\infty}\big[\Xi_3^{[1]-}(k_1)E\big(i\mathbf{k}_S^{[1]-}\cdot\mathbf{x}\big) + \Xi_3^{[1]+}(k_1)E\big(\mathbf{k}_S^{[1]+}\cdot\mathbf{x}\big)\big]\mathrm{d}k_1, \quad (21)$$

wherein (for $\omega \geq 0$)

$$\mathbf{k}_P^{[l]\pm} = \big(k_1, k_{P2}^{[l]\pm}\big), \quad k_{P2}^{[l]\pm} = \pm\sqrt{\big(k_P^{[l]}\big)^2 - (k_1)^2},$$
$$\Re\sqrt{\big(k_P^{[l]}\big)^2 - (k_1)^2} \geq 0, \quad \Im\sqrt{\Big(k_P^{[l]}\Big)^2 - (k_1)^2} \geq 0, \quad (22)$$

$$\mathbf{k}_S^{[l]\pm} = \big(k_1, k_{S2}^{[l]\pm}\big), \quad k_{S2}^{[l]\pm} = \pm\sqrt{\big(k_S^{[l]}\big)^2 - (k_1)^2},$$
$$\Re\sqrt{\big(k_S^{[l]}\big)^2 - (k_1)^2} \geq 0, \quad \Im\sqrt{\big(k_S^{[l]}\big)^2 - (k_1)^2} \geq 0, \quad (23)$$

with

$$k_P^{[l]} = \frac{\omega}{c_P^{[l]}} = \frac{\omega}{\sqrt{\frac{\lambda^{[l]}+2\mu^{[l]}}{\rho^{[l]}}}}, \quad E\big(\mathbf{k}_\Pi^{[l]\pm}\cdot\mathbf{x}\big) := \exp\big(i\mathbf{k}_\Pi^{[l]\pm}\cdot\mathbf{x}\big); \quad \Pi = P, S, \quad (24)$$

and $c_P^{[l]}$ the phase velocity of compressional body waves in $M^{[l]}$.

Note that these field representations involve nine unknown functions $\Phi^{[0]+}$, $\Psi^{[0]+}$, $\Xi^{[0]+}$, $\Phi^{[1]-}$, $\Psi^{[1]-}$, $\Xi^{[1]-}$, $\Phi^{[1]+}$, $\Psi^{[1]+}$, $\Xi^{[1]+}$. The latter will be obtained by applying the nine boundary conditions embodied in (4)–(12).

2.2.4. *Application of the boundary condition(s)*

The use of (4), (6), (7), (9), (10), and (12), in (16)–(24) gives rise to

$$\Phi^{[0]+} = \Psi_3^{[0]+} = \Phi^{[1]-} = \Psi_3^{[1]-} = \Phi^{[1]+} = \Psi_3^{[1]+} = 0, \quad \Xi_3^{[1]-} = \Xi_3^{[1]+} := A^{[1]}; \quad \forall k_1 \in \mathbb{R}. \quad (25)$$

hence

$$u^{[1]}(\mathbf{x}) = 2\int_{-\infty}^{\infty} A^{[1]}(k_1)\cos\big(k_2^{[1]}x_2\big)\exp(ik_1x_1)\mathrm{d}k_1 =; \quad \forall\mathbf{x}\in\Omega_1, \quad (26)$$

$$u^{[0]d}(\mathbf{x}) = \int_{-\infty}^{\infty} A^{[0]+}(k_1)\exp\big(ik_2^{[0]+}x_2\big)\exp(ik_1x_1)\mathrm{d}k_1 =; \quad \forall\mathbf{x}\in\Omega_0, \quad (27)$$

wherein

$$k_2^{[l]} := k_{S2}^{[l]+}; \quad l = 0, 1, \quad k_2^i := k_{S2}^{i+} = -k_2^{i-}. \quad (28)$$

The use of (26) and (27) together with (8) and (11), followed by Fourier inversion, leads to

$$A^{[0]+}(k_1) = \mathcal{R}^{[0]}(k_1)A^{i-}\delta(k_1 - k_1^i), \quad A^{[1]}(k_1) = \frac{1}{2}\mathcal{R}^{[1]}(k_1)A^{i-}\delta(k_1 - k_1^i), \quad (29)$$

wherein: $\delta(\ )$ is the Dirac delta distribution and

$$\mathcal{R}^{[0]}(k_1) = \left[\frac{\mu^{[0]}k_2^i \cos\left(k_2^{[1]}h\right) + i\mu^{[1]}k_2^{[1]} \sin\left(k_2^{[1]}h\right)}{\mu^{[0]}k_2^i \cos\left(k_2^{[1]}h\right) - i\mu^{[1]}k_2^{[1]} \sin\left(k_2^{[1]}h\right)}\right] \exp\left[-i\left(k_2^i + k_2^{[0]}\right)h\right], \tag{30}$$

$$\mathcal{R}^{[1]}(k_1) = \left[\frac{\mu^{[0]}k_2^{[0]} + \mu^{[0]}k_2^i}{\mu^{[0]}k_2^i \cos\left(k_2^{[1]}h\right) - i\mu^{[1]}k_2^{[1]} \sin\left(k_2^{[1]}h\right)}\right] \exp(-ik_2^i h). \tag{31}$$

2.2.5. *The total fields in the two media*

The consequence of all this is that

$$u_1^{[l]}(\mathbf{x}, \omega) = u_2^{[l]}(\mathbf{x}, \omega) = 0; \quad \forall \mathbf{x} \in \Omega_l; \ l = 0, 1, \tag{32}$$

$$u_3^{[0]}(\mathbf{x}, \omega) = u_3^{[0]-}(\mathbf{x}, \omega) + u_3^{[0]+}(\mathbf{x}, \omega); \quad \forall \mathbf{x} \in \Omega_0, \tag{33}$$

wherein

$$u_3^{0-}(\mathbf{x}, \omega) = u_3^i(\mathbf{x}, \omega) = A^{i-} e^{i[k_1^i x_1 - k_2^{[0]i} x_2]}, \tag{34}$$

$$u_3^{[0]+}(\mathbf{x}, \omega) = \mathcal{R}^{[0]}(k_1^i) A^{i-} e^{i[k_1^i x_1 + k_2^{[0]i} x_2]}, \tag{35}$$

and

$$u_3^{[1]}(\mathbf{x}, \omega) = u_3^{[1]-}(\mathbf{x}, \omega) + u_3^{[1]+}(\mathbf{x}, \omega); \quad \forall \mathbf{x} \in \Omega_1 \tag{36}$$

wherein

$$u_3^{[1]-}(\mathbf{x}, \omega) := \frac{\mathcal{R}^{[1]}(k_1^i)}{2} A^{i-} e^{i[k_1^i x_1 - k_2^{[1]i} x_2]}, \tag{37}$$

$$u_3^{[1]+}(\mathbf{x}, \omega) := \frac{\mathcal{R}^{[1]}(k_1^i)}{2} A^{i-} e^{i[k_1^i x_1 + k_2^{[1]i} x_2]}, \tag{38}$$

with (for $\omega \geq 0$)

$$\begin{gathered} k_2^{[l]i} := \sqrt{(k^{[l]})^2 - (k_1^i)^2}, \quad \Re k_2^{[l]i} \geq 0, \quad \Im k_2^{[l]i} \geq 0, \\ l = 0, 1 \quad \left(k_1^i = k^{[0]} \sin\theta_S^i, \ k_2^i = k_2^{[0]i}\right). \end{gathered} \tag{39}$$

These results, together with (14), indicate that the total fields in Ω_0 and Ω_1 have the same (SH) polarization as the incident field.

2.2.6. *Numerical results for the frequency domain response on the ground*

From (36)–(38), we obtain

$$\frac{u_3^{[1]}(0, 0, \omega)}{2} = u_3^{1\pm}(0, 0, \omega) = \frac{\mathcal{R}^{[1]}(k_1^i)}{2} A^{i-}(\omega) = A^{i-}(\omega) \frac{i}{D(k_1^i)}, \tag{40}$$

wherein

$$D(k_1^i) = ia\cos(\gamma\omega) + b\sin(\gamma\omega), \tag{41}$$

$$a = 1, \quad b = b(\omega, s^i) = \frac{\mu^{[1]}(\omega)\kappa^{[1]i}(\omega, s^i)}{\mu^{[0]}\kappa^{[0]i}(s^i)}, \quad \gamma(\omega, s^i) = \kappa^{[1]i}(\omega, s^i)\frac{h}{c_S^{[0]}}, \tag{42}$$

$$\kappa^{[l]i} := \frac{k_2^{[l]i}}{k^{[0]}} = \sqrt{[c_S^{[0]}/c_S^{[l]}(\omega)]^2 - (s^i)^2}, \quad s^i := \frac{k_1^i}{k^{[0]}}. \tag{43}$$

Henceforth, we assume that the body wave strikes the layer/substratum interface at normal incidence so that $s^i = 0$.

Moreover, we shall be concerned with excitation by a seismic signal in the form of a Ricker pulse. The amplitude spectrum (or frequency domain amplitude) $A^{i-}(\omega)$ of this pulse [2] is

$$A^{i-}(\omega) = -\mathcal{A}\frac{1}{\sqrt{\pi}}\frac{\omega^2}{4\alpha^3}\exp\left(i\beta\omega - \frac{\omega^2}{4\alpha^2}\right), \tag{44}$$

wherein $\mathcal{A}$, α and β are real constants (i.e. independent of ω).

In Figure 2, we plot the spectrum ($A^{i-}(\omega)$) of a Ricker pulse excitation, the transfer function $u_3^{[1]}(0, 0, \omega)/2A^i(\omega)$, and the spectrum of a typical displacement response $u_3^{[1]}(0, 0, \omega)/2$.

2.3. *Time domain analysis of the reflection of a SH plane body wave from a stress-free planar boundary overlying a soft layer underlain by a hard substratum*

2.3.1. *Time history of a Ricker pulse plane body wave propagating in free space*

On account of (1), the time history of solicitation is

$$\begin{aligned} u_3^i(\mathbf{x}, t) &= \int_{-\infty}^{\infty} A^{i-}(\omega)\exp[-i\omega\tau(\mathbf{x}, t, s^i)]\mathrm{d}\omega \\ &= \mathcal{A}\left[-1 + 2\alpha^2\{\tau(\mathbf{x}) - \beta\}^2\right]\exp[-\alpha^2\{\tau(\mathbf{x}, t, s^i) - \beta\}^2], \end{aligned} \tag{45}$$

wherein

$$\tau(\mathbf{x}, t, s^i) = t - \frac{x_1}{c_S^{[0]}}s^i + \frac{x_2}{c_S^{[0]}}c^i. \tag{46}$$

Thus, the Ricker pulse plane body wave attains its maximum (in absolute value) at $\tau(\mathbf{x}, t, s^i) = \beta$, and the main lobe of the pulse is all the narrower the larger is α.

2.3.2. *Time history of the reflected and transmitted plane body wave pulses in the basement and layer*

Recall that $k^{[l]} = \omega/c_S^{[l]}$. We encountered previously, in connection with the frequency domain response in Ω_0 and Ω_1, plane wave functions of the type

$$u_3^{[l]\pm}(\mathbf{x}, \omega) = \mathcal{R}^j(s^i, \omega)A^{i-}(\omega)\exp\left[i\omega\left(s^i\frac{x_1}{c_S^{[0]}} \pm \kappa^{[l]i}\frac{x_2}{c_S^{[0]}}\right)\right]; \quad l = 0, 1, \tag{47}$$

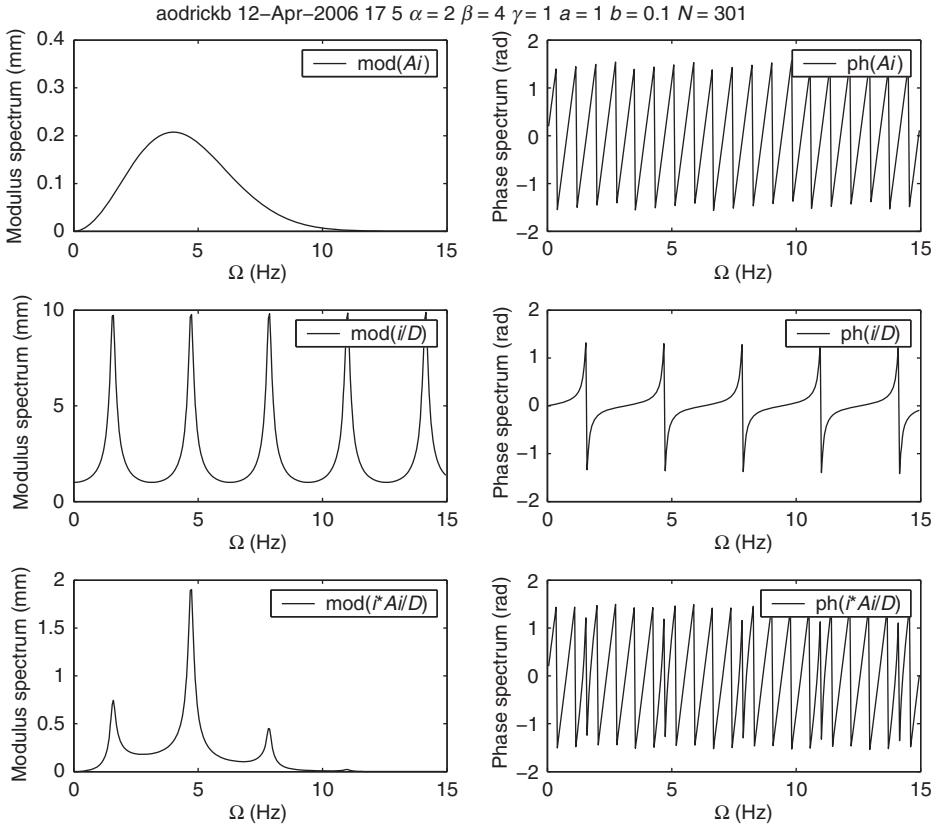

Figure 2. Spectrum of displacement response at $\mathbf{x}=(0,0)$. $\mathcal{A}=1$, $\alpha=2$, $\beta=4$, $\gamma=1$, $a=1$, $b=0.1$, corresponding to a case of merged pulses. The left-hand curves pertain to moduli, and the right hand curves to phases of the spectra. The top panels depict A^{i-}, the middle panels i/D, and the lower panels iA^i/D.

wherein (recall that we assumed that $c_S^{[0]}$ does not depend on ω) $\kappa^{[l]i}=\sqrt{[c_S^{[0]}/c_S^{[l]}(\omega)]^2-(s^i)^2}$.

Let

$$\mathcal{R}^{[0]}(\omega,s^i)=R^{[0]}(\omega,(s^i)e^{\left[-2i\kappa^{0i}(s^i)\frac{h}{c_S^{[0]}}\right]},\quad \mathcal{R}^{[1]}(\omega,s^i)=R^{[1]}(\omega,(s^i)e^{\left[-i\kappa^{0i}(s^i)\frac{h}{c_S^{[0]}}\right]}. \tag{48}$$

Thus, by virtue of (1), the time history of the fields in the basement and layer are:

$$u_3^{[0]+}(\mathbf{x},t)=\int_{-\infty}^{\infty}A^{i-}(\omega)R^{[0]}(\omega,s^i)\exp\left[-i\omega\tau^{[0]+}(\mathbf{x},t,s^i)\right]\mathrm{d}\omega, \tag{49}$$

$$u_3^{[1]\pm}(\mathbf{x},t)=\int_{-\infty}^{\infty}A^{i-}(\omega)\frac{R^{[1]}(\omega,s^i)}{2}\exp\left[-i\omega\tau^{[1]\pm}(\mathbf{x},t,\omega,s^i)\right]\mathrm{d}\omega, \tag{50}$$

wherein

$$\tau^{[0]+}(\mathbf{x},t,s^i):=t-s^i\frac{x_1}{c_S^{[0]}}-\kappa^{0i}(s^i)\frac{x_2}{c_S^{[0]}}+2\kappa^{0i}(s^i)\frac{h}{c_S^{[0]}}, \tag{51}$$

$$\tau^{[1]\pm}(\mathbf{x}, t, \omega, s^i) := t - s^i \frac{x_1}{c_S^{[0]}} \mp \kappa^{1i}(\omega, s^i) \frac{x_2}{c_S^{[0]}} + \kappa^{0i}(s^i) \frac{h}{c_S^{[0]}}. \tag{52}$$

In the following, whenever numerical results are given, they will apply to the field on the ground at point $\mathbf{x} = (0,0)$.

Recall that the time domain displacement response in the layer is of the form $u_3^{[1]}(\mathbf{x}, t) = u_3^{[1]-}(\mathbf{x}, t) + u_3^{[1]+}(\mathbf{x}, t)$, so that

$$\frac{u_3^{[1]}(0, 0, t)}{2} = u_3^{[1]\pm}(0, 0, t). \tag{53}$$

It is this function, related to the *temporal displacement response on the ground*, that will be depicted in the graphs that are presented further on.

2.3.2. *Evaluation of $u_3^{[1]\pm}(\mathbf{x}, t)$ for Ricker pulse excitation by the complex frequency pole-residue convolution scheme*

The time history of the displacement field in Ω_1 is of the form

$$\begin{aligned} u_3^{[1]\pm}(\mathbf{x}, t) &= \int_{-\infty}^{\infty} A^{i-}(\omega) \frac{R^{[1]}(\omega, s^i)}{2} \exp\left[-i\omega\tau^{[1]\pm}(\mathbf{x}, t, \omega, s^i)\right] \mathrm{d}\omega \\ &= i \int_{-\infty}^{\infty} \frac{A^{i-}(\omega)}{D(\omega, s^i)} \exp\left[-i\omega\tau^{[1]\pm}(\mathbf{x}, t, \omega, s^i)\right] \mathrm{d}\omega, \end{aligned} \tag{54}$$

wherein

$$D(\omega, s^i) = ia\cos(\gamma\omega) + b\sin(\gamma\omega), \tag{55}$$

$$a = 1, \quad b = b(\omega, s^i) = \frac{\mu^{[1]}(\omega)\kappa^{[1]i}(\omega, s^i)}{\mu^{[0]}\kappa^{[0]i}(s^i)}, \quad \gamma(\omega, s^i) = \kappa^{[1]i}(\omega, s^i) \frac{h}{c_S^{[0]}}. \tag{56}$$

The task is thus to evaluate the Fourier integral of a product of two functions F_1 and F_2

$$u(t) = \int_{-\infty}^{\infty} F_1(\omega) F_2(\omega) \exp(-i\omega\tau) \mathrm{d}\omega, \quad F_2(\omega) = A^{i-}(\omega), \quad F_1(\omega) = \frac{i}{D(\omega, s^i)}. \tag{57}$$

It is easily shown that

$$u(t) = \frac{1}{2\pi} \int_0^{\infty} [F_1(-t_1) F_2(t + t_1) + F_1(t_1) F_2(t - t_1)] \mathrm{d}t_1, \tag{58}$$

wherein $F_1(t)$ and $F_2(t)$ are the Fourier transforms of $F_1(\omega)$ and $F_2(\omega)$, respectively.

We now apply this formula to evaluate the time history of response. As mentioned above, we assume that *the media are dispersionless*, so that $\tau^{[1]\pm}(\mathbf{x}, t, \omega, s^i) = \tau^{[1]\pm}(\mathbf{x}, t, s^i)$, hence

$$u_3^{[1]\pm}(\mathbf{x}, t) = \frac{1}{2\pi} \int_0^{\infty} \left[F_1(-t_1) F_2\left(\tau^{[1]\pm}(\mathbf{x}, t, s^i) + t_1\right) + F_1(t_1) F_2\left(\tau^{[1]\pm}(\mathbf{x}, t, s^i) - t_1\right)\right] \mathrm{d}t_1. \tag{59}$$

The Fourier inverse of $F_2(\omega)$ was given in (45) and the Fourier inverse of $F_1(\omega)$ is

$$F_1(t_1) = \int_{-\infty}^{\infty} \frac{i}{D(\omega, s^i)} \exp(-i\omega t_1) \mathrm{d}\omega. \tag{60}$$

Assuming, as before, that b is real, we note immediately that although the denominator of the integral in (60) does not vanish for *real* ω, it can vanish for *complex* ω. This suggests that the integral can be evaluated via the Cauchy theorem by appealing to a suitable integration path in the complex ω plane. Actually D vanishes at an infinite number of locations in the complex $\omega = \omega' + \omega''$ plane, so that we rather proceed as following.

In order to stress the fact that the integration variable in (60) is real (i.e. ω'), and for other reasons, we re-write the integral as

$$F_1(t) = \int_{-\infty}^{\infty} \frac{i}{D(\omega', s^i)} \exp(-i\omega t) \mathrm{d}\omega', \tag{61}$$

wherein $D(\omega', s^i) = ia\cos(\gamma\omega') + b\sin(\gamma\omega')$. We assume that D vanishes at a denumerable set of *complex* frequencies $\{\omega_m; m \in \mathbb{Z}\}$, i.e. $D(\omega_m, s^i) = 0$; $m \in \mathbb{Z}$. This suggests expanding $D(\omega, s^i)$ in a Taylor series around $\omega = \omega_m$:

$$D(\omega, s^i) = D(\omega_m, s^i) + (\omega - \omega_m)\dot{D}(\omega_m, s^i) + \cdots, \tag{62}$$

wherein

$$\dot{D}(s^i, \omega_m) = \frac{\partial D(\omega, s^i)}{\partial \omega}\bigg|_{\omega=\omega_m} = \dot{D}(\omega_m, s^i). \tag{63}$$

We adopt the approximation

$$\frac{1}{D(\omega', s^i)} \approx \frac{1}{(\omega' - \omega_m)\dot{D}(\omega_m, s^i)}. \tag{64}$$

Now, let us turn to the issue of the actual locations of the zeros of D. We search for the complex roots ω of

$$D(\omega, s^i) = ia\cos(\gamma\omega) + b\sin(\gamma\omega) = ia\cos(\gamma(\omega' + i\omega'')) + b\sin(\gamma(\omega' + i\omega'') = 0, \tag{65}$$

and assume, as was implicit (or explicitly stated), that a, b and γ are real (this being notably the case, assumed herein, in which the media (basement and layer) are non-lossy. Then

$$\begin{aligned} D(\omega, s^i) &= \sin(\gamma\omega')[a\sinh(\gamma\omega'') + b\cosh(\gamma\omega'')] + i\cos(\gamma\omega')[a\cosh(\gamma\omega'') + b\sinh(\gamma\omega'')] \\ &= 0, \end{aligned} \tag{66}$$

or, owing to the fact that we have a mixture of real and complex quantities,

$$\sin(\gamma\omega')[a\sinh(\gamma\omega'') + b\cosh(\gamma\omega'')] = 0, \tag{67}$$

$$\cos(\gamma\omega')[a\cosh(\gamma\omega'') + b\sinh(\gamma\omega'')] = 0. \tag{68}$$

Moreover, a, b and γ do not depend on ω due to the fact that it was assumed that $\mu^{[l]}$ and $c^{[l]}$ do not depend on ω. Consequently, we have two families of solutions, the first of which corresponds to

$$\sin(\gamma\omega') = 0, \quad a\cosh(\gamma\omega'') + b\sinh(\gamma\omega'') = 0, \tag{69}$$

and the second of which corresponds to

$$\cos(\gamma\omega') = 0, \quad a\sinh(\gamma\omega'') + b\cosh(\gamma\omega'') = 0. \tag{70}$$

The (so-called *even*) solutions of the first family are:

$$\omega_m^{e'} = \frac{m\pi}{\gamma}, \quad \omega_m^{e''} = \frac{1}{2\gamma}\ln\left(\frac{b-a}{b+a}\right); \quad m \in \mathbb{Z}, \tag{71}$$

and the (so-called *odd*) solutions of the second family are

$$\omega_m^{o'} = \frac{(2m+1)\pi}{2\gamma}, \quad \omega_m^{o''} = \frac{1}{2\gamma}\ln\left(\frac{a-b}{a+b}\right); \quad m \in \mathbb{Z}. \tag{72}$$

The question is whether we have to deal with either even or odd solutions. We can show that

$$b^2 \gtrless a^2 \Leftrightarrow \frac{\mu^{[1]}\rho^{[1]}}{\mu^{[0]}\rho^{[0]}} - \left(\frac{\mu^{[1]}}{\mu^{[0]}}s^i\right)^2 \gtrless \left[1-(s^i)^2\right]. \tag{73}$$

But $0 \le |s^i| \le 1$, so that for $s^i = 0$ (i.e. normal incidence):

$$b^2 \gtrless a^2 \Leftrightarrow \mu^{[1]}\rho^{[1]} \gtrless \mu^{[0]}\rho^{[0]}, \tag{74}$$

whereas for $s^i = \pm 1$ (i.e. grazing incidence)

$$b^2 \gtrless a^2 \Leftrightarrow \rho^{[1]} \gtrless \rho^{[0]}. \tag{75}$$

In the (geophysical) case of interest herein, i.e. dealing with a soft layer overlying a hard substratum, we have $\mu^{[0]} > \mu^{[1]}$ and $\rho^{[0]} > \rho^{[1]}$, so that we are clearly in the situation $b < a$ for all incidence angles. *This situation is that of odd solutions*.

Consequently, the time history of displacement in the layer is

$$F_1(t) \approx i\sum_{m\in\mathbb{Z}} \frac{1}{\dot{D}(\omega_m^o, s^i)} \int_{-\infty}^{\infty} \frac{1}{\omega' - \omega_m^o} \exp(-i\omega' t)\mathrm{d}\omega'. \tag{76}$$

The evaluation of the integral

$$\mathcal{I}(\mathbf{x}, t) = \int_{-\infty}^{\infty} \frac{1}{\omega' - \omega_m^o} \exp(-i\omega t)\mathrm{d}\omega', \tag{77}$$

wherein $\omega_m^{o''} < 0$; $\forall m \in \mathbb{Z}$ (which means that the pole of the integrand lies in the lower half part of the complex ω plane for all $m \in \mathbb{Z}$), is carried out by the method of residues to yield [3]

$$\mathcal{I}(\mathbf{x}, t) = -2\pi i \exp(-i\omega_m^o t)H(t), \tag{78}$$

wherein H is the Heaviside distribution ($H(\chi) = 0$; $\chi < 0$ and $H(\chi) = 1$; $\chi > 0$).

It follows from (60) that

$$F_1(t_1) = 2\pi \sum_{m\in\mathbb{Z}} \frac{\exp(-i\omega_m^o t_1)}{\dot{D}(\omega_m^o, s^i)} H(t_1), \tag{79}$$

hence

$$u_3^{[1]\pm}(\mathbf{x}, t) = \frac{1}{2\pi}\int_0^\infty F_1(t_1) F_2\big(\tau^{[1]\pm}(\mathbf{x}, t, s^i) - t_1\big)\mathrm{d}t_1, \tag{80}$$

or, more explicitly,

$$\begin{aligned} u_3^{[1]\pm}(\mathbf{x}, t) = \mathcal{A} \sum_{m\in\mathbb{Z}} \frac{1}{\dot{D}(\omega_m^o, s^i)} \int_0^\infty \big[-1 + 2\alpha^2(\tau^{[1]\pm}(\mathbf{x}, t, s^i) - t_1 - \beta)^2\big] \\ \times \exp[-i\omega_m^o t_1 - \alpha^2(\tau^{[1]\pm}(\mathbf{x}, t, s^i) - t_1 - \beta)^2]\mathrm{d}t_1. \end{aligned} \tag{81}$$

Knowing that

$$\dot{D}(\omega_m^o, s^i) = i(-1)^m \gamma \frac{b^2 - a^2}{a} \cosh(\gamma\omega_m^{o''}) = i(-1)^m \dot{\mathrm{D}}(s^i), \quad \dot{\mathrm{D}}(s^i) = \gamma \frac{b^2 - a^2}{a} \cosh(\gamma\omega^{o''}), \tag{82}$$

we observe that $\omega_m^{o''} = \omega^{o''}$ and $\dot{\mathrm{D}}(s^i)$ are independent of m. Thus, we can write (81) as

$$\begin{aligned} u_3^{[1]\pm}(\mathbf{x}, t) = \frac{\mathcal{A}}{i\dot{\mathrm{D}}} \int_0^\infty S(t_1)\big[-1 + 2\alpha^2(\tau^{[1]\pm}(\mathbf{x}, t, s^i) - t_1 - \beta)^2\big] \\ \times \exp[-i\omega_m^o t_1 - \alpha^2(\tau^{[1]\pm}(\mathbf{x}, t, s^i) - t_1 - \beta)^2]\mathrm{d}t_1, \end{aligned} \tag{83}$$

wherein

$$S(t_1) = \sum_{m=-\infty}^{\infty} (-1)^m \exp(-i\omega_m^o t_1) = \exp(\omega^{o''} t_1) \sum_{m=-\infty}^{\infty} (-1)^m \exp\left[-i(2m+1)\frac{\pi}{2\gamma} t_1\right]. \tag{84}$$

Thus

$$\begin{aligned} u_3^{[1]\pm}(\mathbf{x}, t) = \frac{\mathcal{A}}{i\dot{\mathrm{D}}} \int_0^\infty \sigma(t_1)\big[-1 + 2\alpha^2(\tau^{[1]\pm}(\mathbf{x}, t, s^i) - t_1 - \beta)^2\big] \\ \times \exp[\omega^{o''} t_1 - \alpha^2(\tau^{[1]\pm}(\mathbf{x}, t, s^i) - t_1 - \beta)^2]\mathrm{d}t_1, \end{aligned} \tag{85}$$

wherein

$$\sigma(t_1) = \sum_{m=-\infty}^{\infty} (-1)^m \exp\left[-i(2m+1)\frac{\pi}{2\gamma} t_1\right] = \exp\left(-i\frac{\pi}{2\gamma} t_1\right) \sum_{m=-\infty}^{\infty} \exp\left[i\frac{m\pi}{\gamma}(\gamma - t_1)\right]. \tag{86}$$

We make use of the *Poisson sum formula* [3] to obtain

$$\sum_{m=-\infty}^{\infty} \exp\left[i\frac{m\pi}{\gamma}(\gamma - t_1)\right] = 2\gamma \sum_{m=-\infty}^{\infty} \delta(\gamma - t_1 + 2m\gamma) = 2\gamma \sum_{m=-\infty}^{\infty} \delta(t_1 - (2m+1)\gamma). \tag{87}$$

But (recall that $\gamma > 0$) $t_1 = (2m+1)\gamma < 0$ for $m < 0$, so that

$$\sigma(t_1) = 2\gamma \exp\left(-i\frac{\pi}{2\gamma}t_1\right)\sum_{m=0}^{\infty}\delta(t_1 - (2m+1)\gamma); \quad t_1 \geq 0. \tag{88}$$

Consequently,

$$u_3^{[1]\pm}(\mathbf{x}, t) = \frac{-2i\gamma\mathcal{A}}{i\dot{\mathrm{D}}}\sum_{m=0}^{\infty}(-1)^m\int_0^{\infty}\delta(t_1 - (2m+1)\gamma)\left[-1 + 2\alpha^2(\tau^{[1]\pm}(\mathbf{x}, t, s^i) - t_1 - \beta)^2\right]$$
$$\times \exp[\omega^{o''}t_1 - \alpha^2(\tau^{[1]\pm}(\mathbf{x}, t, s^i) - t_1 - \beta)^2]\mathrm{d}t_1, \tag{89}$$

or finally, on account of the sifting property of the Dirac delta distribution,

$$u_3^{[1]\pm}(\mathbf{x}, t) = \frac{-2\gamma\mathcal{A}}{\dot{\mathrm{D}}}\sum_{m=0}^{\infty}(-1)^m\left[-1 + 2\alpha^2\{\tau^{[1]\pm}(\mathbf{x}, t, s^i) - (2m+1)\gamma - \beta\}^2\right]$$
$$\times \exp[\omega^{o''}(2m+1)\gamma - \alpha^2\{\tau^{[1]\pm}(\mathbf{x}, t, s^i) - (2m+1)\gamma - \beta\}^2]. \tag{90}$$

The terms of the series decrease exponentially with increasing m so that the series can be approximated by a sum of $M+1$ terms

$$u_3^{[1]\pm}(\mathbf{x}, t) \approx \frac{-2\gamma\mathcal{A}}{\dot{\mathrm{D}}}\sum_{m=0}^{M}(-1)^m\left[-1 + 2\alpha^2\{\tau^{[1]\pm}(\mathbf{x}, t, s^i) - (2m+1)\gamma - \beta\}^2\right]$$
$$\times \exp[\omega^{o''}(2m+1)\gamma - \alpha^2\{\tau^{[1]\pm}(\mathbf{x}, t, s^i) - (2m+1)\gamma - \beta\}^2], \tag{91}$$

which is the form adopted in the numerical applications of this method.

Remark As shown in [4], the complex frequency method gives rise to the correct solution in all cases of geophysical interest.

2.3.3. *Numerical results for ground response to Ricker pulse normally-incident body wave solicitation*

The temporal domain ground response corresponding to the frequency domain ground response of Figure 2 is depicted in Figure 3.

3. The inverse-scattering problem

3.1. *Statement of the inverse problem*

We saw above that a temporal response is an integral I which is a function of the physical and geometrical parameters of the geophysical structure and of the seismic solicitation. We term these parameters $a, \alpha, b, \beta, c, \gamma, \ldots$. The forward scattering problem was to compute $I(a, \alpha, b, \beta, c, \gamma, \ldots, \mathbf{x}, t)$ for different combinations of $a, \alpha, b, \beta, c, \gamma, \ldots$. The inverse scattering problem is to recover one or several of the parameters $a, \alpha, b, \beta, c, \gamma, \ldots$ from data pertaining to the signal $I(a, \alpha, b, \beta, c, \gamma, \ldots, \mathbf{x}, t)$.

Herein, the parameters are b, α, β, γ and we wish to recover the rigidity contrast parameter b from the response signal $I(b, \alpha, \beta, \gamma, (0,0), t)$; $t \in [0, T]$.

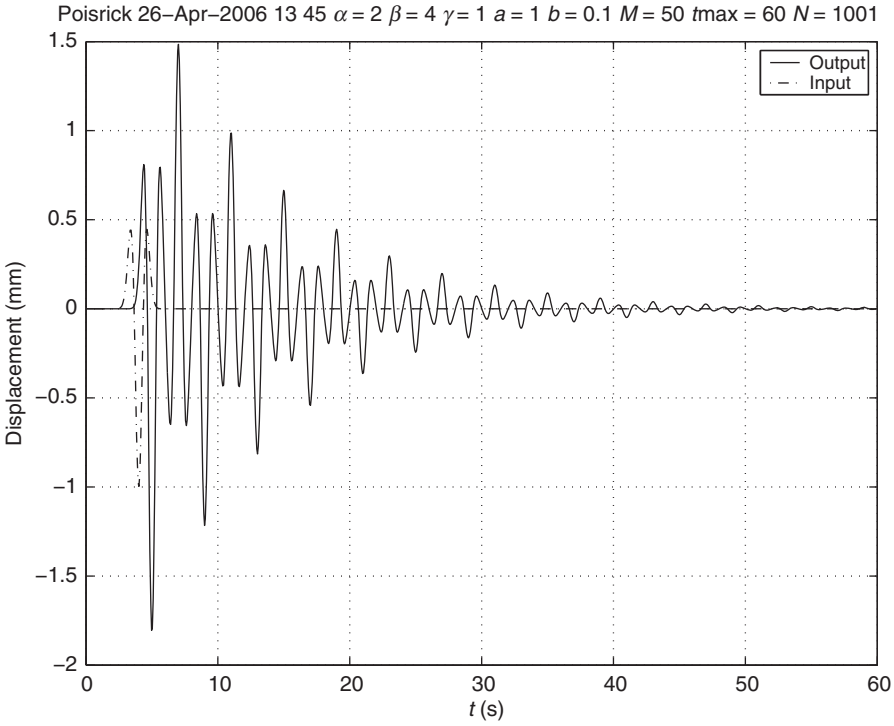

Figure 3. Time history of solicitation (dashed curve) and response (continuous curve) displacement at $\mathbf{x} = (0, 0)$ computed by the complex eigenfrequency method for merged pulses. $\mathcal{A} = 1$, $\alpha = 2$, $\beta = 4$, $\gamma = 1$, $a = 1$, $b = 0.1$, $M = 50$.

A word is here in order concerning the relation of b and γ to the physical parameters of the scattering configuration. Let $c := c^{[0]}/c^{[1]}$, $\mu := \mu^{[1]}/\mu^{[0]}$, $H := h/c^{[0]}$ and recall that $s^i = \sin\theta_S^i$. Then

$$\gamma = H\sqrt{c^2 - (s^i)^2}, \quad b = \mu\frac{\sqrt{c^2 - (s^i)^2}}{\sqrt{1 - (s^i)^2}}, \tag{92}$$

whence

$$c = \sqrt{\left(\frac{\gamma}{H}\right)^2 + (s^i)^2}, \quad \mu = b\frac{H}{\gamma}\sqrt{1 - (s^i)^2}. \tag{93}$$

At normal incidence (the case assumed henceforth), $s^i = 0$, so that

$$c = \frac{\gamma}{H}, \quad \mu = b\frac{H}{\gamma} = \frac{b}{c}. \tag{94}$$

This shows why, for a normally-incident body wave, the rigidity contrast μ can be obtained from the parameter b.

3.2. *Cost functions*

A cost (or objective) function gives a measure of the discrepancy between a measured quantity and a model of this quantity. The measured quantity incorporates true values of certain parameters whereas the model quantity incorporates trial values of the same parameters. When the cost function attains a minimum, it is hoped that the trial values are as close as possible to the actual values of the parameters. It is during the (iterative) process of inversion that the trial parameters are (iteratively) adjusted so as to minimize the cost function.

In the present setting, the measured quantity (predictor) is the complex frequency evaluation of $I(b, \alpha, \beta, \gamma, (0,0), t)$; $t \in [0, T]$ and the model (estimator) is again the complex frequency evaluation of the same function with trial values B, α, β, Γ respectively. We call the model function $I(B, \alpha, \beta, \Gamma, (0,0), t)$; $t \in [0, T]$. Ideally, we should obtain, at the end of the inversion process, $B = b$.

The cost function we adopt is of the least squares variety and is experessed by

$$\mathcal{K}(B) = \frac{1}{T}\int_0^T [I(b, \alpha, \beta, \gamma, (0,0), t) - I(B, \alpha, \beta, \Gamma, (0,0), t))]^2 \mathrm{d}t. \tag{95}$$

In reality, the signal is discretized, so as to lead to the alternate definition of the cost function

$$\mathcal{K}(B) = \frac{1}{T}\sum_{n=1}^{N} [I(b, \alpha, \beta, \gamma, (0,0), t_n) - I(B, \alpha, \beta, \Gamma, (0,0), t_n))]^2, \tag{96}$$

wherein N is the total number of measurements at the discrete instants t_n in the interval $[0, T]$.

Note that if one employs the same technique (also meaning that all but the sought-for parameter, amongst the parameters on which depend the predictor and estimator, are the same) for computing the estimator as the predictor then one commits the 'inverse crime' [5]. It is then obvious that $\mathcal{K}$ attains at least one minimum when $B = b$, i.e. the inverse problem possesses the 'trivial solution' corresponding to B being strictly equal to b. In the more usual situation, when the model is different from the measurement, as is the case when at least one (other than the sought-for) parameter, amongst the parameters on which depend the predictor and estimator, are different) the outcome of inversion is, at best, $B \approx b$. It is shown in [5] that the closeness of the reconstruction of B to b is related to the closeness of the estimator to the predictor.

3.3. *Inversion*

The inverse problem is to obtain the unknown parameter(s) by minimization of the cost function. Assuming once again that it is b one wants to reconstruct,

$$b = \arg\min_B \mathcal{K}(B). \tag{97}$$

Inversion is the iterative process by which this minimum is found. A primitive, but nonetheless illustrative, way to carry out this inversion is by plotting the cost function on the y-axis versus B on the x-axis so that the value of B, for which $\mathcal{K}$ is visually or numerically found to be minimum, is b.

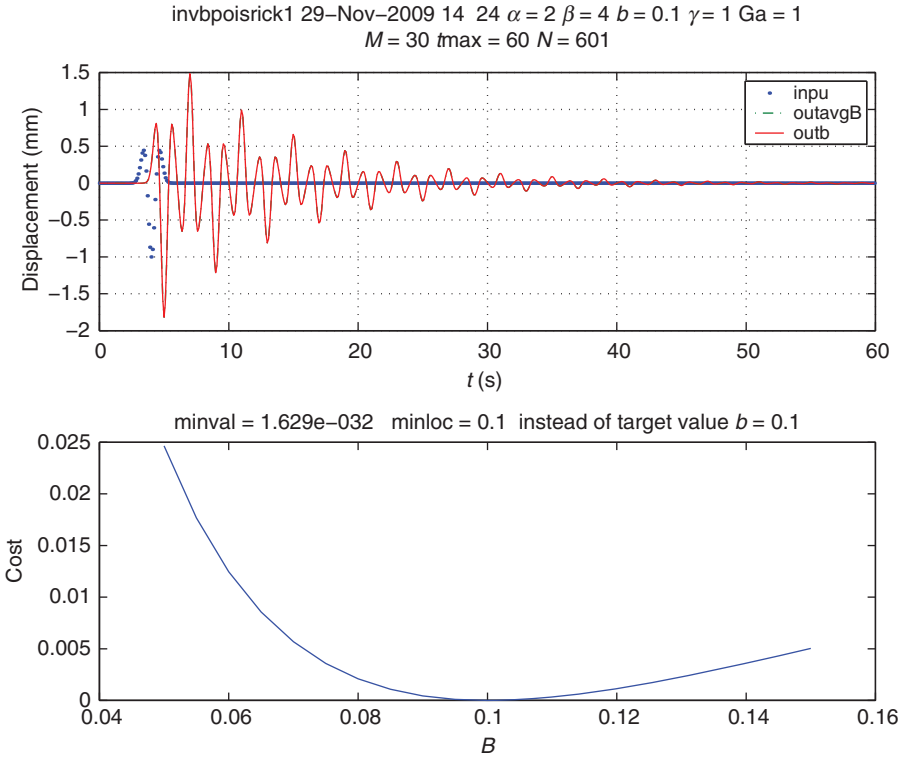

Figure 4. Upper panel: input signal (dotted curve), average output signal employed in the estimator (dashed curve), true output signal employed as the predictor (continuous curve). Lower panel: cost as a function of the trial parameter B. $\alpha=2$, $\beta=4$, $b=0.1$, $\gamma=1$, $\Gamma=1$, $M=30$, $T=60$, $N=1201$.

It should be stressed that *the cost function may possess more than one minima*. Moreover, the deepest minimum may turn out not to correspond to the value of B closest to b. Thus, inversion does not necessarily lead to a unique 'solution', nor to the correct solution.

3.4. *Numerical results for the cost function*

All the following results rely on the complex eigenfrequency method for the computation of the ground temporal response $I = u_3^{[1]}(0,0,t)$ employed in both the predictor and estimator. In all the figures, $\mathcal{A}=1$ and $a=1$. The graphs shown hereafter apply to variations of Γ, T, N for three types of response.

When $\Gamma=\gamma$, the inverse crime is committed. When $\Gamma\neq\gamma$, the inverse crime is not committed because the estimator is not identical to the predictor. If the inversion is correct, we should find that the position of the global minimum of the cost function coincides with the value of b. As is seen below, this is indeed the case when the inverse crime is committed, but not the case otherwise.

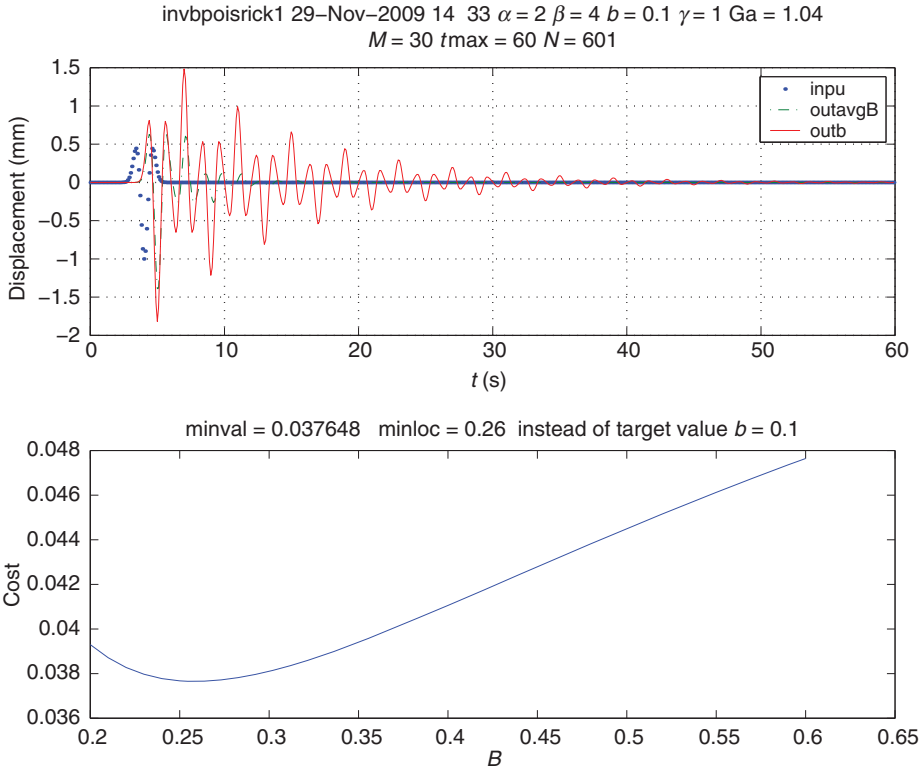

Figure 5. Upper panel: input signal (dotted curve), average output signal employed in the estimator (dashed curve), true output signal employed as the predictor (continuous curve). Lower panel: cost as a function of the trial parameter B. $\alpha = 2$, $\beta = 4$, $b = 0.1$, $\gamma = 1$, $\Gamma = 1.04$, $M = 30$, $T = 60$, $N = 601$.

Figures 4–9 apply to the configuration for which $\alpha = 2$, $\beta = 4$, $b = 0.1$, $\gamma = 1$. In Figures 4–6, we vary the data/model mismatch by varying Γ for a constant, rather wide, time window of measurements. The effect of this variation on the accuracy of the reconstruction of b is illustrated in Figure 7.

In Figures 6, 8 and 9, we vary the time window of measurements for a substantial data/model mismatch ($\gamma = 1$, $\Gamma = 0.96$).

4. Conclusions

Knowing that the complex eigenfrequency method is suitable for evaluating the temporal response of a great variety of scattering configurations [4] of geophysical interest, we have applied it as both the predictor and estimator in order to solve the inverse scattering problem of the recovery of the single parameter b (note that even by employing one or the other of the remaining two methods evaluated in [4] for the predictor would not really avoid committing the inverse crime since it was shown in [6,7] that the three methods give rise to identical results).

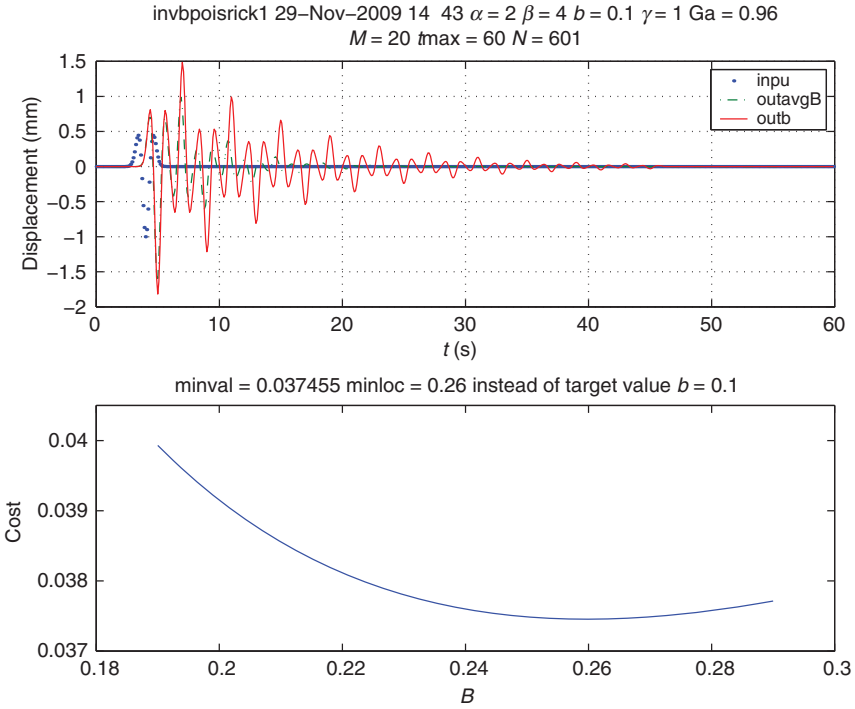

Figure 6. Upper panel: input signal (dotted curve), average output signal employed in the estimator (dashed curve), true output signal employed as the predictor (continuous curve). Lower panel: cost as a function of the trial parameter B. $\alpha = 2$, $\beta = 4$, $b = 0.1$, $\gamma = 1$, $\Gamma = 0.96$, $M = 20$, $T = 60$, $N = 601$.

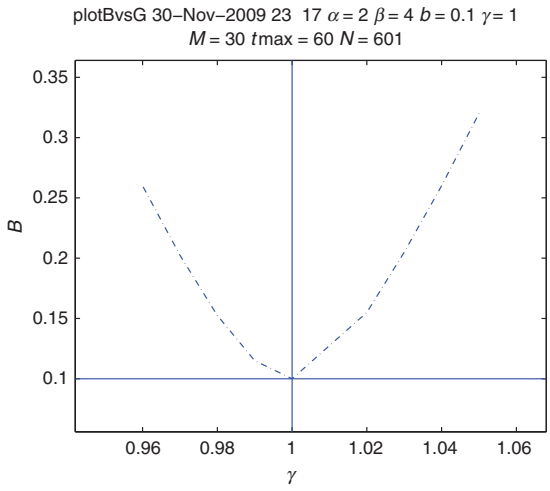

Figure 7. Plot of B versus Γ. The vertical line is $\Gamma = \gamma$, the horizontal line is $B = b$, and their point of intersection corresponds to the inverse crime. Note that the departure from this point of the dot-dashed curve translates the rapidly-diminishing accuracy of the reconstruction of b with increasing predictor/estimator mismatch (regulated by Γ). $\alpha = 1$, $\beta = 4$, $b = 0.1$, $\gamma = 1$, $M = 30$, $T = 60$, $N = 601$.

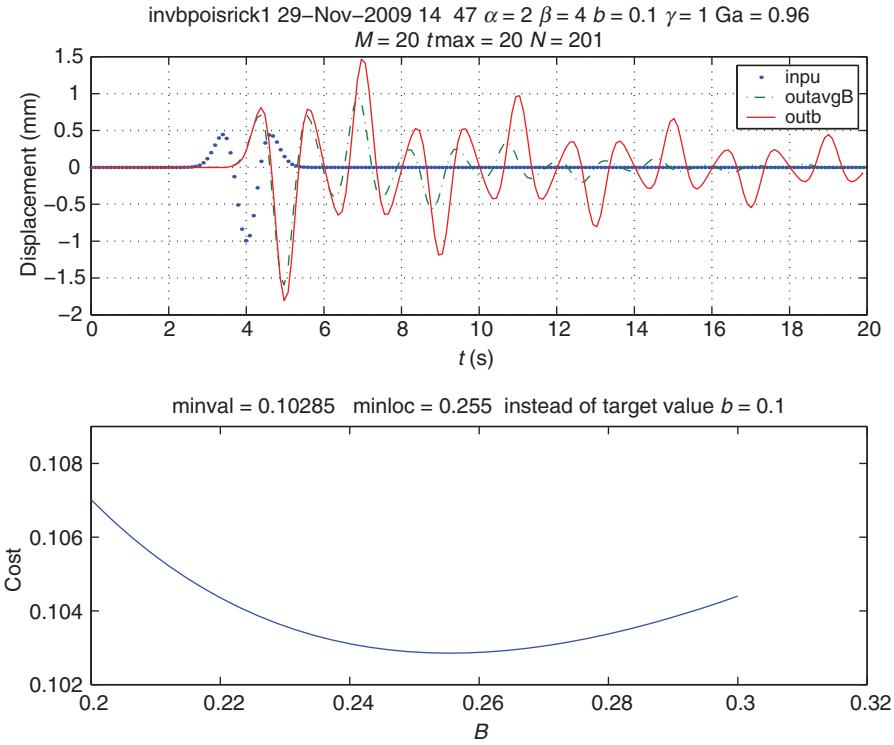

Figure 8. Upper panel: input signal (dotted curve), average output signal employed in the estimator (dashed curve), true output signal employed as the predictor (continuous curve). Lower panel: cost as a function of the trial parameter B. $\alpha = 2$, $\beta = 4$, $b = 0.1$, $\gamma = 1$, $\Gamma = 0.96$, $M = 20$, $T = 20$, $N = 201$.

We have introduced a mismatch between the predictor and estimator taking γ in the former and Γ in the latter, with Γ increasingly-different from γ. This has been shown to lead to an increasing difference of the estimated B from b. An important, although not altogether unexpected, result is that even *a small mismatch between the predictor and estimator leads to a rather large departure of the reconstructed parameter from its target value*. This shows that it is very important to employ models of the wave/scattering configuration interaction which account as accurately as possible for the measured response. If such a model is not available, then the resolution of the inverse problem will either not be solved at all, or be solved with unacceptably-large error.

A somewhat surprising result is that increasing the width of the time window for data acquisition can worsen the estimation of b when there exists a significant mismatch between the estimator and predictor. Note that generally speaking, predictor/estimator response mismatch was found to be smallest in the initial part of the response signal and largest in the coda. Thus, it seems that the best strategy is to employ data that includes only the earliest arrivals, but even this strategy will not

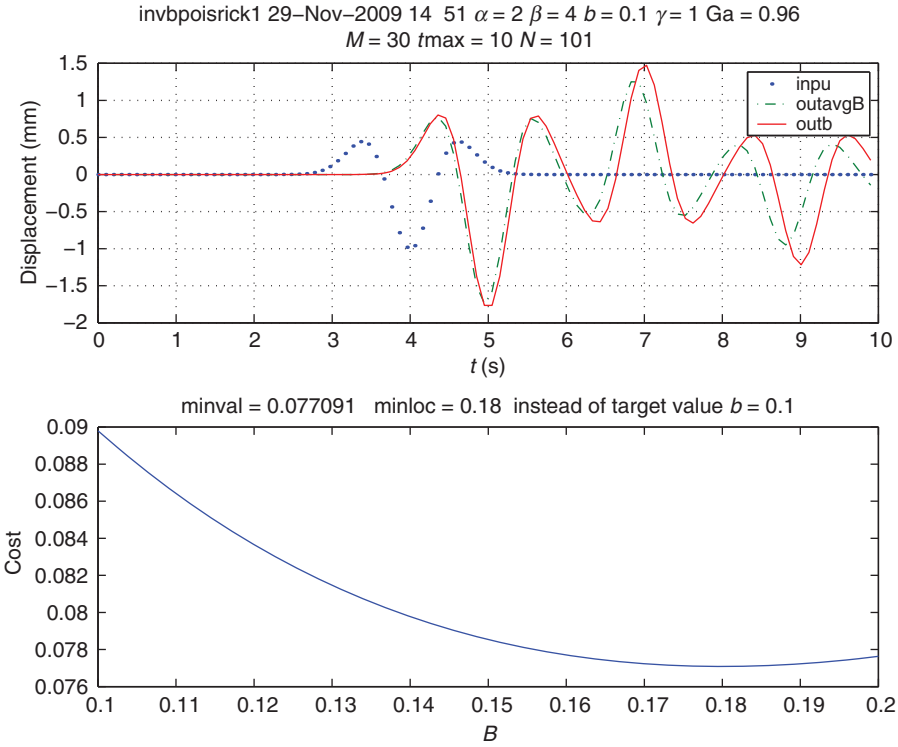

Figure 9. Upper panel: input signal (dotted curve), average output signal employed in the estimator (dashed curve), true output signal employed as the predictor (continuous curve). Lower panel: cost as a function of the trial parameter B. $\alpha = 2$, $\beta = 4$, $b = 0.1$, $\gamma = 1$, $\Gamma = 0.96$, $M = 30$, $T = 10$, $N = 101$.

succeed if the predictor/estimator is large, because then even the early arrival behavior is not well-accounted for by the estimator.

References

[1] J.D. Achenbach, *Wave Propagation in Elastic Solids*, North-Holland, Amsterdam, 1973.
[2] F.J Sanchez-Sesma, *Diffraction of elastic SH waves by wedges*, Bull. Seism. Soc. Am. 75 (1985), pp. 1435–1446.
[3] P.M. Morse and H. Feshbach, *Methods of Theoretical Physics*, Mc Graw-Hill, New York, 1953.
[4] A. Wirgin, Three methods for the description of the temporal response to a SH plane impulsive seismic wave in a soft elastic layer overlying a hard elastic substratum (2006), Available at: http://arxiv.org/abs/physics/0605117
[5] A. Wirgin, The inverse crime (2004). Available at: http://arxiv.org/abs/math-ph/0401050
[6] J.-P. Groby and A. Wirgin, *2D ground motion at a soft viscoelastic layer/hard substratum site in response to SH cylindrical seismic waves radiated by near and distant line sources. I. Theory*, Geophys. J. Int. 163 (2005), pp. 165–191.
[7] J.-P. Groby and A. Wirgin, *2D ground motion at a soft viscoelastic layer/hard substratum site in response to SH cylindrical seismic waves radiated by near and distant line sources. II. Computations*, Geophys. J. Int. 163 (2005), pp. 192–224.